npj | Computational Materials

www.nature.com/npjcompumats

ARTICLE OPEN

Check for updates

A molecular roadmap towards organic donor-acceptor complexes with high-performance thermoelectric response

Wen Shi[1,2], Tianqi Deng[2], Zicong Marvin Wong[2], Gang Wu[2✉] and Shuo-Wang Yang[2✉]

As a unique class of molecular electronic materials, organic donor–acceptor complexes now exhibit tantalizing prospect for heat–electricity interconversion. Over the past decades, in design of these materials for thermoelectric applications, consistent efforts have been made to synthesize a wide variety of structures and to characterize their properties. However, hitherto, one of the paramount conundrums, namely lack of systematic molecular design principles, has not been addressed yet. Here, based on ab initio calculations, and by comprehensively examining the underlying correlation among thermoelectric power factors, non-intuitive transport processes, and fundamental chemical structures for 13 prototypical organic donor–acceptor complexes, we establish a unified roadmap for rational development of these materials with increased thermoelectric response. We corroborate that the energy levels of frontier molecular orbitals in the isolated donor and acceptor molecules control the charge transfer, electronic property, charge transport, and thermoelectric performance in the solid-state complexes. Our results demonstrate that tailoring a suitable energy-level difference between donor's highest occupied molecular orbital and acceptor's lowest unoccupied molecular orbital holds the key to achieving an outstanding power factor. Moreover, we reveal that the charge-transfer-caused Coulomb scattering governs the charge and thermoelectric transport in organic donor–acceptor complexes.

npj Computational Materials (2021)7:107 ; https://doi.org/10.1038/s41524-021-00580-y

INTRODUCTION

The ever-growing need for flexible, low-cost, and eco-friendly wearable power supply and cooling devices has sparked the booming market of organic-based thermoelectric (TE) materials[1,2]. The performance of a TE material is dictated by the dimensionless figure of merit, $zT = \frac{PF}{\kappa}T$, where $PF = S^2\sigma$ is the power factor, S is the Seebeck coefficient, σ is the conductivity, κ is the total thermal conductivity, and T is the temperature[3]. On account of the low thermal conductivity for organic materials, developing organic TE materials with superb power factor lies at the heart of organic TEs[4]. Over the past decades, in pursuit of high-performance organic TE materials, unremitting efforts have been made by materials chemists, solid-state physicists, and device engineers, which has led to extraordinary advances in TE polymers[5,6]. Nowadays, conducting polymers demonstrate room-temperature figures of merit comparable to those of the best conventional inorganic TE materials, strongly guaranteeing them for practical commercial uses[7–9]. However, development of high-efficiency small-molecule organic TE materials is still a formidable challenge.

Organic donor–acceptor complexes are a unique and emerging class of small-molecule organic electronic materials. In recent years, their fascinating prospect for field-effect transistors, photovoltaics, and TEs has stimulated considerable research interests[10]. Organic donor–acceptor complexes consist of two or more molecules and the intermolecular forces drive the aggregation of these isolated molecules, forming regular mixed or segregated stacking arrangement and thereby crystalline solid[11]. Importantly, their diversity in combination of donor and acceptor brings about the versatile and tunable properties.

A series of prominent experimental progress on organic donor–acceptor complexes has corroborated their feasibility for TE applications. The first significant milestone was achieved in single-crystal (TTF)(TCNQ) (TTF = tetrathiofulvalene; TCNQ = tetracyano-*p*-quinodimethane) and it was proven to possess extraordinarily high conductivity (~652 S cm^{-1}) at room temperature using a four-probe method[12]. Recently, it was reported that (BTBT)(F_6TCNNQ) and (CBZ)(F_6TCNNQ) (BTBT = benzo[*b*]benzo[4,5]thieno[2,3-*d*]thiophene; F_6TCNNQ = 1,3,4,5,7,8-hexafluoro-11,11,12,12-tetracyano-2,6-naphthoquinodimethane; CBZ = carbazole) cocrystals show decent room-temperature mobility exceeding 1 cm^2 V^{-1} s^{-1} based on space-charge limited current measurements[13]. Furthermore, the measured power factor of complex (DPTTA)(F_4TCNQ) (DPTTA = meso-diphenyl tetrathia[22]annulene[2,1,2,1]; F_4TCNQ = 2,3,5,6-tetrafluoro-7,7,8,8-tetracyanoquinodimethane) was reported to be 0.33 μW m^{-1} K^{-2} at 300 K[14].

Thorough understandings of structure–function relations are the fountain of efficient materials design. Previous experimental explorations on charge transport and TE properties in organic donor–acceptor complexes mainly focus on the preparation of materials and performance characterization. Nevertheless, one of the current unsolved major puzzles is the lack of systematic materials design guidelines for this rising class of systems, and knowing very little about the basic structure–property relationships and the fundamental physical processes is the root cause of this problem. To deal with these issues, we herein carry out comprehensive first-principles computational investigations on the TE properties of 13 prototypical organic donor–acceptor complexes by using density functional theory, Boltzmann transport equation, Brooks–Herring approach, and deformation potential (DP) theory. We create an intuitive and general molecular roadmap for rational design of organic donor–acceptor complexes with high-performance TE response and, concurrently, we provide a unified understanding of correlation among their power factors, nontrivial physical processes, and elementary chemical structures.

[1]School of Chemistry, Sun Yat-sen University, Guangzhou, China. [2]Institute of High Performance Computing, Agency for Science, Technology and Research, Singapore, Republic of Singapore. ✉email: wug@ihpc.a-star.edu.sg; yangsw@ihpc.a-star.edu.sg

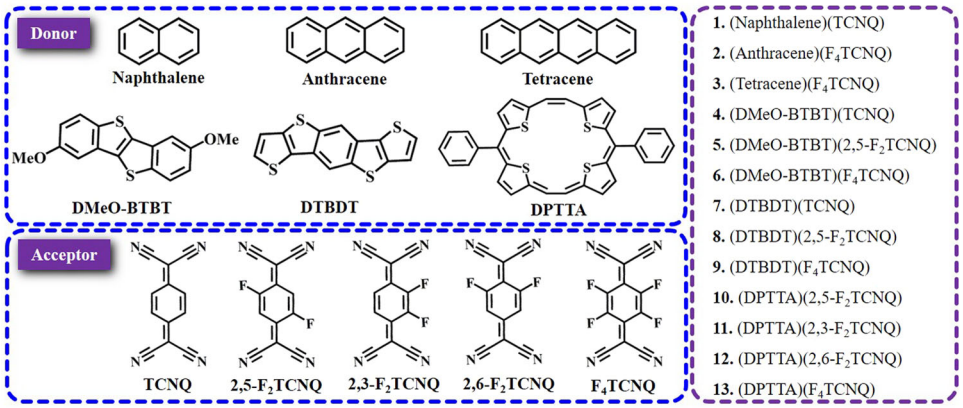

Fig. 1 Chemical structures of our studied six donor molecules and five acceptor molecules. The number and abbreviation of our studied 13 organic donor–acceptor complexes are also displayed in the figure. Their full name, source of crystallographic structures, and lattice parameters are shown in Supplementary Table 1 and their crystalline structures are displayed in Supplementary Fig. 1.

RESULTS AND DISCUSSIONS

Charge transport and TE response performance

The 13 representative organic donor–acceptor complexes with well-defined crystallographic structures are explored (Fig. 1 and Supplementary Table 1). In order to make our results general, the donors that make up these complexes exhibit various molecular structures. Among them, naphthalene, anthracene, and tetracene are composed of the linearly fused benzene rings; 3,8-dimethoxy-[1]benzothieno[3,2-*b*][1]benzothiophene (DMeO-BTBT) and dithieno[2,3-d;2′3′-*d*′]benzo[1,2-*b*;4,5-*b*′]dithiophene (DTBDT) contain the fused thiophene and benzene rings; DPTTA consists of the cyclic extended conjugated moiety and the phenyl group. For the acceptors, the five ubiquitous fluorinated derivatives of 7,7,8,8-tetracyanoquinodimethane (F_nTCNQ, $n = 0$, 2, 4) are involved. Moreover, this series of organic donor–acceptor complexes adopt the typical mixed stacking motifs with 1 : 1 stoichiometry along the π–π stacking direction (Supplementary Fig. 1).

Here, Boltzmann transport theory[15,16], combining the DP theory[17], Brooks–Herring approach[18], and density functional electronic structure calculations, is utilized to quantify the charge transport and TE properties for these complexes. The detailed computational methods are summarized in "Methods" section and Supplementary Information. It can be observed from Fig. 2a, b that the evaluated room-temperature hole mobilities for this series of materials fall in the range of 0.004–1.5 $cm^2 V^{-1} s^{-1}$ and their calculated electron mobilities are in the range of 0.07–5 $cm^2 V^{-1} s^{-1}$, implying the superior electron transport for these complexes. It is worth noting that our predicated mobilities are consistent with the state-of-the-art available experimental results (Fig. 2c, d). For instance, the calculated hole mobility for crystalline (DPTTA)(2,5-F_2TCNQ) (**10**) is 1.49 $cm^2 V^{-1} s^{-1}$, quantitatively agreeing with the two experimental values (1.25[19] and 1.01 $cm^2 V^{-1} s^{-1}$[14]) based on the single-crystal field-effect measurements (Fig. 2c). Furthermore, the computed electron mobility (0.051 $cm^2 V^{-1} s^{-1}$) for crystalline (DMeO-BTBT)(2,5-F_2TCNQ) (**5**) is close to the two measured results (0.033 and 0.024 $cm^2 V^{-1} s^{-1}$)[20] by using the single-crystal transistors.

In addition, we notice that the experimental work reports that the measured field-effect electron mobility for the (DPTTA)(F_2TCNQ) single crystal is 0.27 $cm^2 V^{-1} s^{-1}$ at room temperature[14]. However, another experimental study demonstrates that the measured field-effect electron mobility for the (DPTTA)(F_2TCNQ) single crystal is 0.47 $cm^2 V^{-1} s^{-1}$ at room temperature[19]. In fact, the charge transport in a realistic material is very complex. As an example, the previous work has proven that the position disorder for fluorine can exist in F_2TCNQ[19]. We show that the calculated room-temperature electron mobilities for the (DPTTA)(2,5-F_2TCNQ) (**10**), (DPTTA)(2,3-F_2TCNQ) (**11**), and (DPTTA)(2,6-F_2TCNQ) (**12**) are 1.35, 0.77, and 0.54 $cm^2 V^{-1} s^{-1}$, respectively (Fig. 2b), indicating the obvious position disorder effect on mobility. Besides, many other factors (such as grain boundary, defect, dielectric materials, electric field, charge injection, interface effect, etc.) can further attenuate the mobility, thus leading to the difference between the experimental and computational results[19].

Figure 2e–g display the TE transport coefficients for this series of materials, including Seebeck coefficient, conductivity, and power factor. Interestingly, for these organic donor–acceptor complexes, their TE properties vary with the different combinations of donors and acceptors, clearly suggesting their tunable and controllable TE performance. Usually, for organic-based TE materials, achieving the continuous regulation of their transport coefficients, such as via chemical doping[21], field-effect modulation[22], and applying external pressure[23], is critical to optimize their performance. Our results demonstrate that the diversity in combination of donor and acceptor provide a feasible route to continuously tune the TE transport coefficients, thus refining their performance.

Among these organic donor–acceptor complexes, (tetracene)(F_4TCNQ) (**3**), (DPTTA)(2,5-F_2TCNQ) (**10**), (DPTTA)(2,3-F_2TCNQ) (**11**), (DPTTA)(2,6-F_2TCNQ) (**12**), and (DPTTA)(F_4TCNQ) (**13**) exhibit the outstanding room-temperature power factors (1–100 μW $m^{-1} K^{-2}$), mainly owing to their high conductivities (4–108 S cm^{-1}) (Fig. 2f, g). In particular, the power factor of (tetracene)(F_4TCNQ) (**3**) can reach up to 55.9 μW $m^{-1} K^{-2}$, comparable with those of some current cutting-edge donor–acceptor complexes, e.g., a series of newly prepared charge-transfer complexes, $(BTBT)_2XF_6$ (BTBT = [1]benzothieno[3,2-b][1]benzothiophene; X = P, As, Sb, and Ta) with the power factor of 55–88 μW $m^{-1} K^{-2}$ (Fig. 2h)[24]. This apparently indicates that by rationally designing the isolated donor and acceptor molecules, and properly combining them, the organic donor–acceptor complexes are capable of showing the remarkable power factor.

Our calculated room-temperature Seebeck coefficients for the (DPTTA)(2,5-F_2TCNQ) (**10**), (DPTTA)(2,3-F_2TCNQ) (**11**), and (DPTTA)(2,6-F_2TCNQ) (**12**) are −45, −64, and −113 μV K^{-1}, respectively. We find that the conduction bands (CBs) for **10**, **11**, and **12** display very narrow dispersions from R_2–U_2 and X–V_2 (Supplementary Fig. 3h–j), which can result in large density of states near band edge; however, their valence bands (VBs) all show very dispersive characteristic, naturally leading to small density of states near band edge. Therefore, for these materials, the electrons contribute more to the Seebeck coefficient, thus giving rise to the negative sign of calculated Seebeck coefficients. The previous works have also confirmed such band structure characteristic for the (DPTTA)

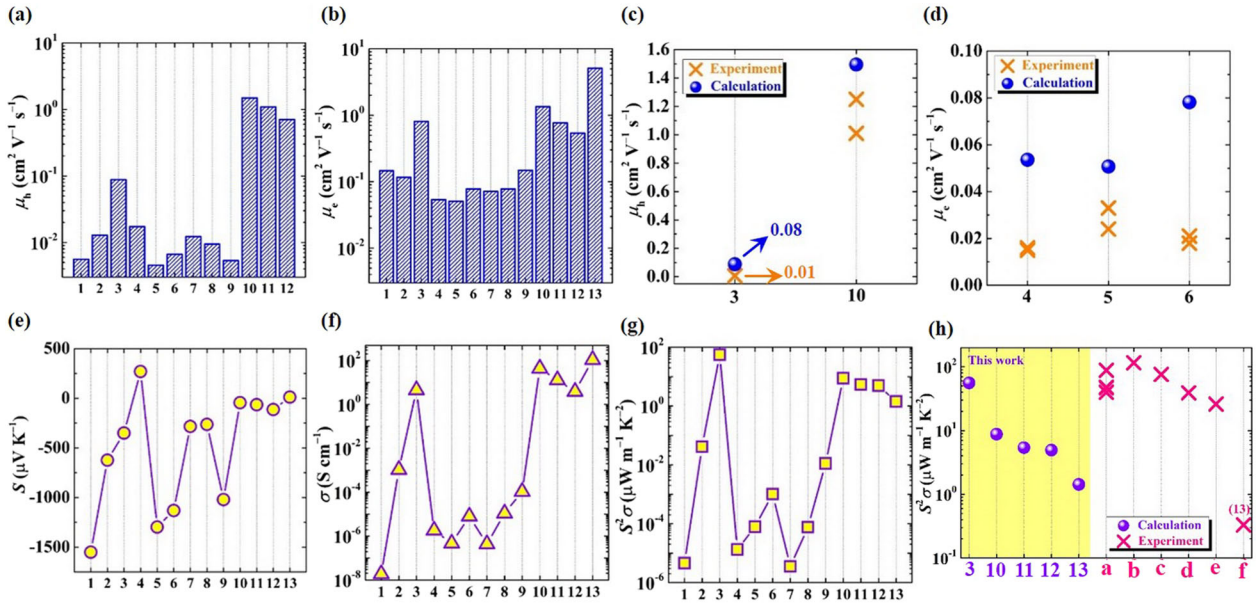

Fig. 2 Charge transport and TE response performance. The calculated **a** hole (μ_h) and **b** electron (μ_e) mobilities at room temperature. **c** The comparison between the calculated hole mobilities (μ_h, circle) and the measured ones (cross). **d** The comparison between the calculated electron mobilities (μ_e, circle) and the measured ones (cross). The calculated **e** Seebeck coefficient (S), **f** conductivity (σ), and **g** power factor ($S^2\sigma$) at room temperature. **h** The calculated power factor ($S^2\sigma$) for the five best materials among our studied systems at room temperature (circle). The measured power factors (cross) for some current advanced donor–acceptor complexes are also displayed in the figure. The compound **a**–**f** stand for $(BTBT)_2XF_6$, $Cu(DMDCNQI)_2$, (TTF)(TCNQ), $(TTM\text{-}TTP)(I_3)_{5/3}$, $(TMTSF)_2PF_6$, and (DPTTA)(F_4TCNQ), respectively, and their full names are shown in Supplementary Table 5. The corresponding references of the published experimental works in **c**, **d**, and **h** are summarized in Supplementary Table 5.

(2,5-F_2TCNQ) (**10**)[14,19]. Furthermore, we prove that the (DPTTA)(F_4TCNQ) (**13**) exhibits very small calculated positive Seebeck coefficient (12 μV K^{-1}) at room temperature, due to its metallic band structure (Fig. 3e). Analogously, the experimental study reports that the $(BTBT)_2XF_6$ shows very small positive room-temperature Seebeck coefficient (15 μV K^{-1}), owing to their metallic band structures[24].

Like mobility, we find that the position disorder for fluorine has an obvious impact on the conductivity. For instance, our calculated conductivities for the (DPTTA)(2,5-F_2TCNQ) (**10**), (DPTTA)(2,3-F_2TCNQ) (**11**), and (DPTTA)(2,6-F_2TCNQ) (**12**) are 44, 13, and 4 S cm^{-1}, respectively, at room temperature (Fig. 2f).

Electronic structure: from molecule to solid-state complexes

To shed light on the underlying interplay between the TE transport properties of the solid-state complexes and the isolated donor and acceptor molecules, we first systematically probe the electronic structures from the isolated molecules to solids. For organic donor–acceptor complexes, charge transfer is a basic and unique characteristic, and it is usually believed that the electrons in the highest occupied molecular orbital (HOMO) of donor can transfer to the lowest unoccupied molecular orbital (LUMO) of acceptor[25]. Figure 3a shows that the donors' HOMO levels of our studied systems vary largely from −6.1 to −4.8 eV, and as the number of the substituted fluorine atoms increases, the acceptor's LUMO levels slightly decrease from −5.1 to −5.6 eV (Supplementary Table 6). Figure 3b and Supplementary Table 7 display that the degree of charge transfer of our studied systems falls in the range of 0–1. More importantly, we find that the charge transfers between the donor and the acceptor in crystalline complexes display a linear relationship with the energy-level difference between donor's HOMO and acceptor's LUMO (Fig. 3b). This observation unambiguously demonstrates that the energy-level difference for the isolated donor and acceptor molecules plays a predominant role in the charge transfer process for the solid-state complexes.

Fig. 3c–e and Supplementary Fig. 3 show the orbital projected band structures for our studied organic donor–acceptor complexes and it is found that except (DPTTA)(F_4TCNQ) (**13**), all the rest of materials (**1**–**12**) are typical semiconductors. Moreover, the metallic band structure of **13** is confirmed by the Heyd–Scuseria–Ernzerhof (HSE06) functional[26] calculations and the supercell electronic structure calculations (see Supplementary Fig. 4 and Supplementary Table 8 for details). The intrinsic metallic characteristic of **13** also satisfactorily interprets its outstanding conductivity (108 S cm^{-1}) (Fig. 2f). Overall, as can be seen from the band structures of this series of materials, by combining the different donor and acceptor, the organic donor–acceptor complexes can exhibit versatile electronic properties (from semiconductor to metal).

To further explore the interplay between the electronic structure and the charge transfer for these complexes, we quantitatively analyze the contributions of the donor and acceptor to the band structure. It is demonstrated from Fig. 3f and Supplementary Table 9 that for **1**–**12**, the VBs and CBs are mainly contributed by the donor and acceptor molecules, respectively. Importantly, we find that as the charge transfer increases, the contributions of donor to the CBs and those of acceptor to the VBs increase (Fig. 3f). Specifically, for (DPTTA)(F_4TCNQ) (**13**), the close-to-unity (0.88e) charge transfer leads to the metallic band structure, and DPTTA and F_4TCNQ make almost 50% contributions to the bands near the Fermi level, which results in its highly dispersive bands (537 meV) (Fig. 3g). These findings clearly evidence that as the charge transfer increases, the charge carriers tend to become more delocalized. Therefore, Fig. 3g shows that as the contributions of donor to the VBs and those of acceptor to the CBs decrease, the band dispersions gradually increase, indicating the enhanced intermolecular electronic coupling. On the basis of these results, we thus conclude that a large energy-level difference between donor's HOMO and acceptor's LUMO gives

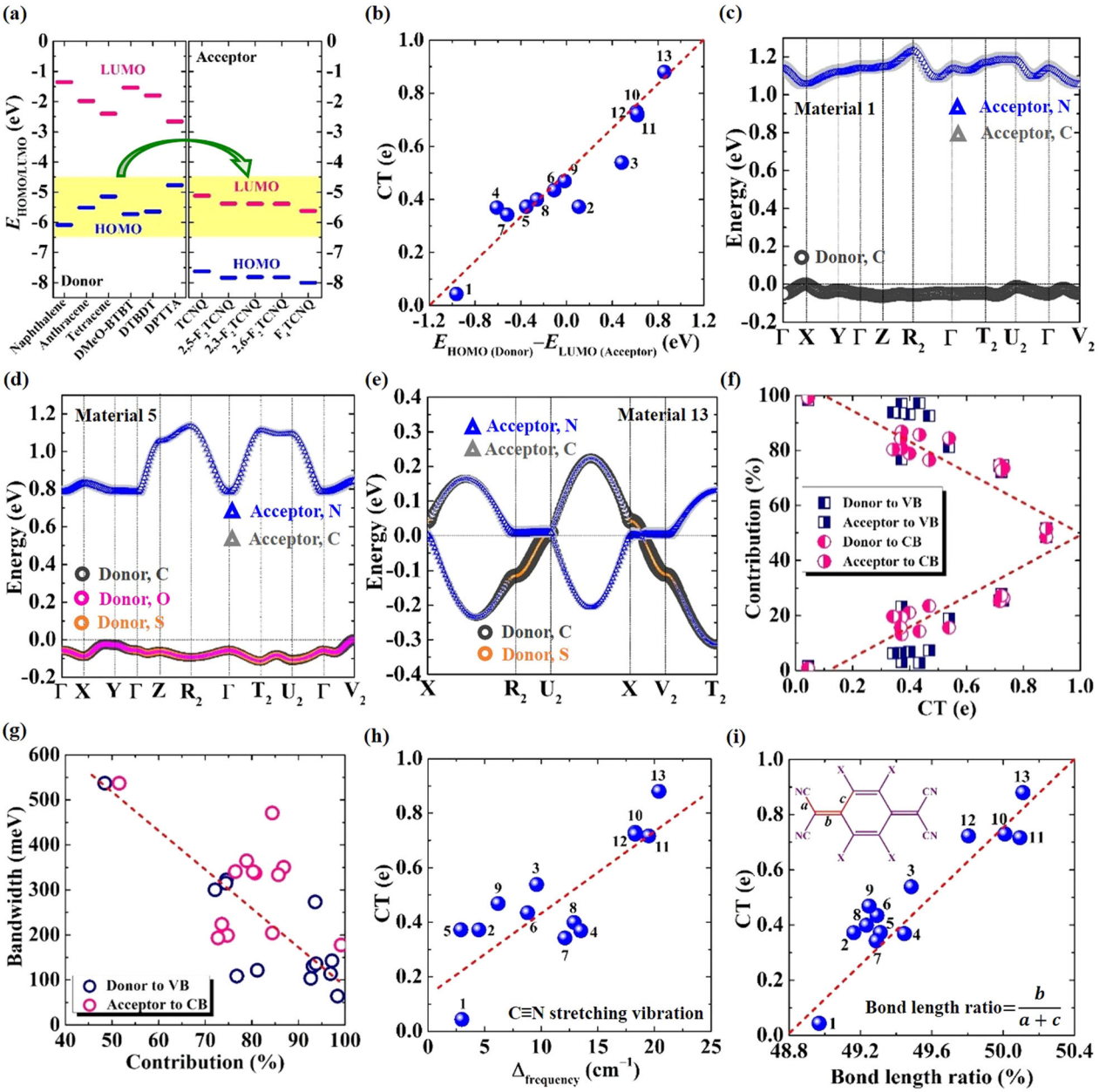

Fig. 3 General correlations among molecular structure, energy level, charge transfer, and electronic structure. a The HOMO (blue) and LUMO (magenta) energy level ($E_{HOMO/LUMO}$) for our studied isolated donor and acceptor molecules. **b** The relationship between the charge transfer (CT) and the energy-level difference ($E_{HOMO(Donor)} - E_{LUMO(Acceptor)}$, where $E_{HOMO(Donor)}$ and $E_{LUMO(Acceptor)}$ are the HOMO energy level of donor and LUMO energy level of acceptor, respectively.). The red dashed line shows the trend. **c**–**e** The orbital projected band structures for (naphthalene)(TCNQ) (**1**), (DMeO-BTBT)(2,5-F_2TCNQ) (**5**), and (DPTTA)(F_4TCNQ) (**13**), respectively. The symbol size denotes the relative weight of the component ratio. The reciprocal coordinates of high-symmetry *k*-points in the first Brillouin zone are $\Gamma = (0, 0, 0)$, $X = (0.5, 0, 0)$, $Y = (0, 0.5, 0)$, $Z = (0, 0, 0.5)$, $R_2 = (-0.5, -0.5, 0.5)$, $T_2 = (0, -0.5, 0.5)$, $U_2 = (-0.5, 0, 0.5)$, and $V_2 = (0.5, -0.5, 0)$, respectively. The carbon, oxygen, and sulfur atoms in the donor molecules are shown in open gray circle, open pink circle, and open orange circle, respectively; the nitrogen and carbon atoms in the acceptor molecules are shown in open blue triangle and open gray triangle, respectively. The orbital projected band structures for other materials are shown in Supplementary Fig. 3. **f** The relationship between the contributions of donor and acceptor to valence band (VB) and conduction band (CB), and the charge transfer (CT). The red dashed line shows the trend. **g** The relationship between the bandwidth and the contributions of donor to VB, and those of acceptor to CB. The red dashed line shows the trend. **h** The relationship between the charge transfer (CT) and the shift of C ≡ N stretching vibrational frequency in acceptor ($\Delta_{frequency}$). The red dashed line shows the trend. **i** The relationship between the charge transfer (CT) and the bond length ratio in acceptor. The definition of bond length ratio is given in the inset. The red dashed line displays the trend.

rise to a large charge transfer, thereby bringing about highly dispersive bands, and even a metallic electronic structure, which implies a good charge transport property. The detailed discussions on the relationship between the charge transport and the energy-level difference between donor's HOMO and acceptor's LUMO will be presented below.

Besides, we demonstrate that the shift of C ≡ N stretching vibrational frequency in acceptor (Fig. 3h) and the bond length

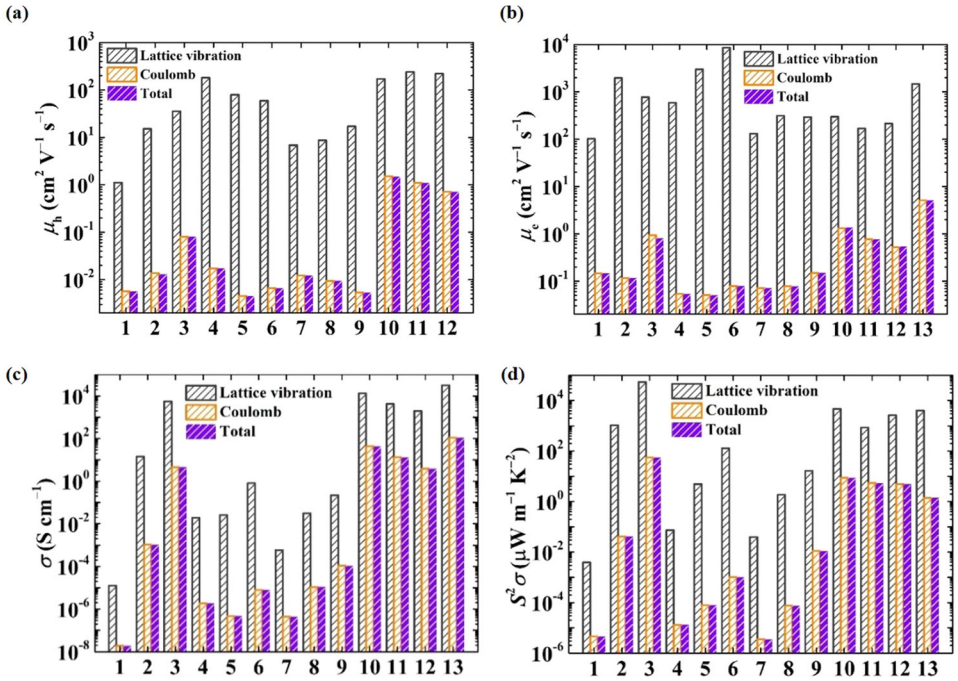

Fig. 4 Competition between the lattice vibration scattering and the Coulomb scattering in the charge and TE transport. The contributions of lattice vibration scattering (dark gray) and those of Coulomb scattering (orange) to the calculated **a** hole mobility (μ_h), **b** electron mobility (μ_e), **c** conductivity (σ), and **d** power factor ($S^2\sigma$) at room temperature for our studied organic donor–acceptor complexes.

ratio defined in Fig. 3i can be used to conveniently characterize the degree of charge transfer in organic donor–acceptor complexes (Supplementary Fig. 6 and Supplementary Table 10). For instance, as the shift of C ≡ N stretching vibrational frequency or the bond length ratio increase, the degree of charge transfer becomes large (Fig. 3h, i). These results suggest that in addition to a large energy-level difference between donor's HOMO and acceptor's LUMO, both a large shift of C ≡ N stretching vibration and a high bond length ratio in acceptor are strong experimentally measurable predictors for a large-degree charge transfer.

Effect of Coulomb scattering on TE performance

As mentioned above, for organic donor–acceptor complexes, charge transfer occurs from the donor to the acceptor, resulting in the positively charged donor and the negatively charged acceptor. In the process of charge and TE transport, due to the electrostatic interactions between the mobile carriers and the ionized donors or acceptors, the charge carriers inevitably undergo Coulomb scattering. Consequently, not only the lattice vibration scattering but also the Coulomb scattering limits the charge dynamics and TE transport in organic donor–acceptor complexes. Deeply understanding the roles of these two scattering processes in the charge and TE transport is crucial to formulate a systematic material design strategy.

Therefore, we herein respectively calculated the TE transport coefficients contributed by the lattice vibration scattering and by the Coulomb scattering, and the computational details can be found in "Methods" section and Supplementary Information. Interestingly, we find that for the studied organic donor–acceptor complexes, the Coulomb scattering rather than the lattice vibration scattering plays a leading role in the hole and electron mobilities, because the evaluated mobilities caused by the Coulomb scattering are at least two orders of magnitude lower than those caused by the lattice vibration scattering, and the formers are much closer to the total mobility (Fig. 4a, b and Supplementary Table 11). Furthermore, as a result of its leading role in the mobility, the Coulomb scattering also dominates the conductivity and thereby the power factor (Fig. 4c, d and Supplementary Table 12).

For organic donor–acceptor complexes, charge transfer from the donor to the acceptor is the origin of the dominant role of Coulomb scattering in the charge and TE transport. Analogously, it has been theoretically unveiled that in the doped π-conjugated polymers, the charge transport and TE properties are governed by the counterion-caused Coulomb scattering, due to the charge transfer from the polymers to the dopants[27–29]. Besides, the agreement between our calculated mobility and the experimental ones (Fig. 2c, d) also corroborates the predominant role of Coulomb scattering in the charge and TE transport. These findings obviously highlight that in organic donor–acceptor complexes, the charge transfer not only controls the static electronic structure, but also markedly impacts on the charge dynamics and TE transport.

Controlling energy levels en route to high TE performance

We have offered a unified understanding on the electronic structure for organic donor–acceptor complexes and, concurrently, we have unveiled a general competitive relationship between the charge-transfer-caused Coulomb scattering and the lattice vibration scattering in their charge and TE transport. We now concentrate on a paramount question: from the perspective of molecular design, what class of organic donor–acceptor complexes exhibit excellent power factor?

Figure 5a shows that for our studied materials, as the energy-level difference between donor's HOMO and acceptor's LUMO increases, both the hole and electron mobilities are elevated; the main reason for such phenomenon is the highly dispersive bands caused by the large charge transfer (Fig. 3). Furthermore, as a result of the enhanced mobility (Fig. 5a), the conductivity is also boosted as such energy-level difference increases (Fig. 5b). These findings evidently indicate that designing the organic donor–acceptor complexes with large energy-level difference between donor's HOMO and acceptor's LUMO is of extreme importance to achieve their remarkable charge transport property.

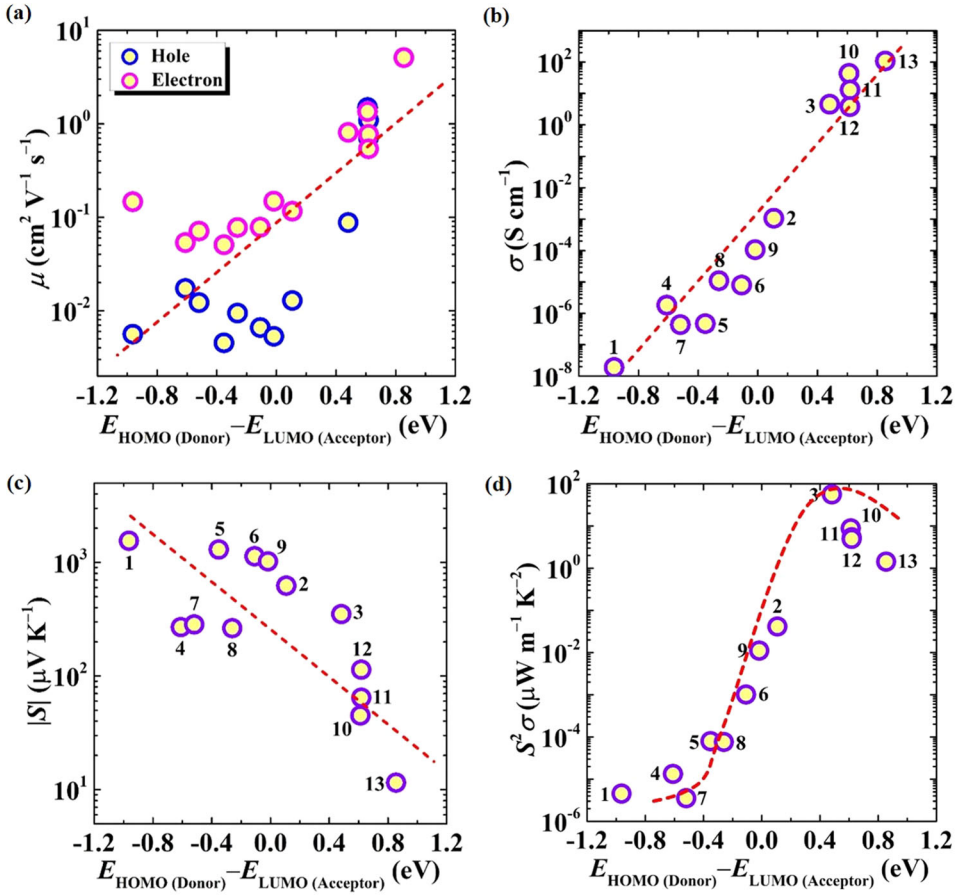

Fig. 5 Enhancing the charge transport and TE performance through engineering the energy levels of frontier molecular orbitals. The dependence of the room-temperature **a** mobility (μ), **b** conductivity (σ), **c** absolute value of Seebeck coefficient ($|S|$), and **d** power factor ($S^2\sigma$) on the energy-level difference ($E_{HOMO(Donor)} - E_{LUMO(Acceptor)}$) for our studied organic donor–acceptor complexes. The red dashed lines exhibit the trend.

Usually, for donor molecule, expanding its π-conjugated backbone can effectively elevate its HOMO level, thus enlarging the energy-level difference with the acceptor's LUMO. As an example, in (DPTTA)(F_4TCNQ) (**13**), the HOMO level of DPTTA with cyclic extended π-conjugated moiety is 0.86 eV higher than the LUMO level of F_4TCNQ (Fig. 3a), which leads to its large-degree charge transfer (0.88e, Fig. 3b), highly dispersive bands (537 meV, Fig. 3g), and thereby outstanding mobility (5.1 cm^2 V^{-1} s^{-1}, Fig. 5a) and conductivity (108 S cm^{-1}, Fig. 5b).

To further prove the critical role of large energy-level difference between donor's HOMO and acceptor's LUMO in the increased conductivity, we examine the relationship between the carrier concentration and the energy-level difference between donor's HOMO and acceptor's LUMO (Supplementary Fig. 7). It is found that there is no obvious correlation between them, which demonstrates that the dominant reason for the increased conductivity is the improved mobility.

Figure 5c demonstrates that as the increased energy-level difference between donor's HOMO and acceptor's LUMO, the absolute values of our calculated Seebeck coefficients decrease, also because of the enhanced charge transfer degree. Thus, for this series of materials, we find that the power factor first gradually increases and then decreases along with the enlarged energy-level difference between donor's HOMO and acceptor's LUMO, and the maximum power factor is achieved near a specific energy-level difference (Fig. 5d). These results evidently reveal that in the development of organic donor–acceptor complexes with high-performance TE response, we need to simultaneously balance the conductivity and the Seebeck coefficient. When their donor's HOMO level is much higher than their acceptor's LUMO level, the complexes can exhibit a high mobility and conductivity, but in that case, their Seebeck coefficient is too poor to attain a remarkable power factor. Hence, to realize an acceptable power factor, the energy level of the donor's HOMO should be higher than that of the acceptor's LUMO, yet a too large energy-level difference is suggested to be avoided. Among our studied organic donor–acceptor complexes, (tetracene)(F_4TCNQ) (**3**) possesses the highest power factor (55.9 μW m^{-1} K^{-2}, Fig. 5d), moderate conductivity (4.6 S cm^{-1}, Fig. 5b), and absolute Seebeck coefficient (350 μV K^{-1}, Fig. 5c) at room temperature, because compared with the naphthalene and the anthracene, the tetracene with four fused benzene rings can properly elevate its HOMO level, accordingly resulting in a suitable energy-level difference with the LUMO of F_4TCNQ (0.48 eV).

Recently, some theoretical studies reveal that the super-exchange effect is of importance in the charge transport of organic donor–acceptor complexes[30]. Previous results obtained by one-dimensional tight-binding model uncover that the strong super-exchange couplings are beneficial to the charge carrier delocalization and thereby good charge transport[31,32]. Moreover, by using density functional calculations and one-dimensional tight-binding model, our previous theoretical work proves that the strong super-exchange couplings lead to not only the delocalized charge carrier but also the small DP constant, which helps to attain long scattering time and high mobility[33]. Our present investigations highlight that controlling a suitable energy-level difference between donor's HOMO and acceptor's LUMO is crucial to

achieving highly dispersive bands and thereby an exceptional charge transport, consistent with the super-exchange picture.

In addition, a recent theoretical work uncovers the origin of abnormal Seebeck effect in the doped conducting polymers. It is revealed that the lightly doping-induced localized polaronic band and the small gap between the localized band and CB (or VB) are two basic conditions for observing the abnormal Seebeck effect[34]. The band structures for our studied materials **1**–**12** exhibit typical semiconductive behavior. The material **13** is metal, but it shows highly dispersive bands without doping-induced localized bands. Consequently, the abnormal Seebeck effect cannot be observed in our studied organic donor–acceptor complexes.

In summary, through systematic atomistic-level investigations on the linkage between the TE performance, nontrivial transport processes, and fundamental molecular structures for a series of emerging organic donor–acceptor complexes, we provide a universal molecular roadmap to efficiently design this class of materials with high-performance TE response. We confirm that the energy levels of frontier molecular orbitals in the isolated donor and acceptor molecules determine the charge transfer, electronic structure, charge transport, and TE performance in the solid-state complexes. It is demonstrated that a proper energy-level difference between donor's HOMO and acceptor's LUMO is of vital importance to a superb power factor. Besides, we prove that the charge-transfer-caused Coulomb scattering plays a dominant role in the charge transport and TE properties. These findings are supported by the recent available experimental studies. We expect that our proposed insightful understanding and materials design guidelines will rationalize the properties of the whole family of organic donor–acceptor complexes, and stimulate systematic development of this class of materials with enhanced TE performance.

METHODS

Electronic structure calculations

The initial crystal structures for our studied organic donor–acceptor complexes were obtained from the published experimental works, and the detailed crystallographic information is summarized in Supplementary Table 1. The atomic positions were relaxed by the Perdew–Burke–Ernzerhof (PBE) exchange-correlation functional[35] with the Grimme's D3 dispersion correction[36] in Vienna Ab initio Simulation Package (VASP)[37]. The optimization details and results by using different dispersion corrections are displayed in Supplementary Information. We calculated the electronic structures by using the projector augmented wave method[38] with the PBE functional[35] in VASP[37]. The cutoff energy was set to be 600 eV and the self-consistent convergence criterion of the total energy was set to be 10^{-5} eV. The interpretation on the cutoff energy and convergence criterion we used is shown in Supplementary Information. The charge transfer calculations were carried out by the Bader charge analysis[39]. The computational details on the charge transfer, electronic structures of isolated donors and acceptors, and orbital projected band structures can be found in Supplementary Information.

Scattering time calculations

Based on the Fermi's Golden rule, the momentum-dependent scattering time ($\tau_{\mathbf{k}}$) can be written as

$$\frac{1}{\tau_{\mathbf{k}}}=\frac{2\pi}{\hbar\Omega}\sum_{\mathbf{k}'}|M(\mathbf{k},\mathbf{k}')|^2\delta(E_{\mathbf{k}}-E_{\mathbf{k}'})(1-\cos\theta), \tag{1}$$

where $\hbar$ is the reduced Planck's constant, Ω is the volume of unit cell, $|M(\mathbf{k},\mathbf{k}')|^2$ is the scattering matrix element, $\delta(E_{\mathbf{k}}-E_{\mathbf{k}'})$ is the Dirac delta function, $E_{\mathbf{k}}$ is the band energy, and θ is the scattering angle between the $\mathbf{k}$ and $\mathbf{k}'$ states. We herein consider both the lattice vibration scattering and the Coulomb scattering. Assuming these two scatterings are independent, and on the basis of Matthiessen's rule, the total scattering time has the form $\frac{1}{\tau_{\mathbf{k}}}=\frac{1}{\tau_{\mathrm{L},\mathbf{k}}}+\frac{1}{\tau_{\mathrm{C},\mathbf{k}}}$, where $\tau_{\mathrm{L},\mathbf{k}}$ and $\tau_{\mathrm{C},\mathbf{k}}$ are the scattering time caused by the lattice vibrations and by the Coulomb interactions, respectively.

DP theory for lattice vibration scattering

The DP theory[17] was employed to characterize the acoustic phonon scattering. In this theory, the scattering matrix element takes the form $|M(\mathbf{k},\mathbf{k}')|^2=\frac{k_BTE_1^2}{C_{ii}}$, where k_B is the Boltzmann constant, E_1 is the DP constant, and C_{ii} ($ii=aa$, bb, and cc) is the elastic constant. Both the DP constant and the elastic constant were attained from first-principles computations and the calculation details are shown in Supplementary Information.

Brooks–Herring approach for Coulomb scattering

The Brooks–Herring approach[18] was used to characterize the Coulomb scattering. The screened Coulomb potential between the ionized donor or acceptor molecules and the free charge carriers has the form

$$V(r)=\frac{q_Ie}{4\pi\varepsilon_r\varepsilon_0 r}\exp\left(-\frac{r}{L_D}\right), \tag{2}$$

where q_I is the charge transfer amount, e is the elementary charge, $L_D=\sqrt{\frac{\varepsilon_r\varepsilon_0k_BT}{e^2N}}$ is the screening length, N is the free carrier concentration, ε_r is the relative permittivity, and ε_0 is the dielectric constant of vacuum. Assuming that there are n_I scattering centers in each unit cell and they scatter the charge carriers independently, the scattering matrix element can be expressed as

$$|M(\mathbf{k},\mathbf{k}')|^2=\frac{n_I(q_Ie)^2}{\Omega(\varepsilon_r\varepsilon_0)^2\left(L_D^{-2}+|\mathbf{k}\prime-\mathbf{k}|^2\right)^2}. \tag{3}$$

Boltzmann transport equation for TE performance calculations

We utilized Boltzmann transport theory[15,40] to evaluate the TE transport coefficients. Based on this theory, the conductivity (σ) and the Seebeck coefficient (S) can be written as

$$\sigma=\frac{e^2}{\Omega}\sum_{\mathbf{k}}\left[-\frac{\partial f_0(E_{\mathbf{k}},E_F,T)}{\partial E_{\mathbf{k}}}\right]\mathbf{v}_{\mathbf{k}}\mathbf{v}_{\mathbf{k}}\tau_{\mathbf{k}}, \tag{4}$$

$$S=\frac{e}{\Omega\sigma T}\sum_{\mathbf{k}}\left[-\frac{\partial f_0(E_{\mathbf{k}},E_F,T)}{\partial E_{\mathbf{k}}}\right](E_{\mathbf{k}}-E_F)\mathbf{v}_{\mathbf{k}}\mathbf{v}_{\mathbf{k}}\tau_{\mathbf{k}}. \tag{5}$$

Here, $\mathbf{v}_{\mathbf{k}}=\frac{1}{\hbar}\nabla_{\mathbf{k}}E$ is the group velocity and it was obtained from the band structure calculations. We computed the mobility (μ) based on the relation $\mu=\frac{\sigma}{eN}$. The TE transport coefficients were evaluated by using the BoltzTraP program[15,41], where the scattering times were attained from the density functional computations. The detailed interpretation on the rationality of Boltzmann transport theory is shown in Supplementary Information. To eliminate the effect of the underestimated bandgaps due to the PBE functional[35] on the TE transport coefficients, in TE performance calculations, we used the bandgaps obtained by the HSE06 functional[26].

DATA AVAILABILITY

Any of the data can be provided by the authors upon email request to the corresponding authors.

CODE AVAILABILITY

Any of the code that we have used for our conclusions can be provided by the authors upon email request to the corresponding authors.

Received: 2 May 2021; Accepted: 22 June 2021;
Published online: 14 July 2021

REFERENCES

1. Russ, B., Glaudell, A., Urban, J. J., Chabinyc, M. L. & Segalman, R. A. Organic thermoelectric materials for energy harvesting and temperature control. *Nat. Rev. Mater.* **1**, 16050 (2016).
2. Wang, Y. et al. Flexible thermoelectric materials and generators: challenges and innovations. *Adv. Mater.* **31**, 1807916 (2019).

3. He, J. & Tritt, T. M. Advances in thermoelectric materials research: looking back and moving forward. *Science* **357**, eaak9997 (2017).
4. Chen, Y., Zhao, Y. & Liang, Z. Solution processed organic thermoelectrics: towards flexible thermoelectric modules. *Energy Environ. Sci.* **8**, 401–422 (2015).
5. Bubnova, O. & Crispin, X. Towards polymer-based organic thermoelectric generators. *Energy Environ. Sci.* **5**, 9345–9362 (2012).
6. Kroon, R. et al. Thermoelectric plastics: from design to synthesis, processing and structure–property relationships. *Chem. Soc. Rev.* **45**, 6147–6164 (2016).
7. Kim, G.-H., Shao, L., Zhang, K. & Pipe, K. P. Engineered doping of organic semiconductors for enhanced thermoelectric efficiency. *Nat. Mater.* **12**, 719–723 (2013).
8. Cheng, H., He, X., Fan, Z. & Ouyang, J. Flexible quasi-solid state ionogels with remarkable Seebeck coefficient and high thermoelectric properties. *Adv. Energy Mater.* **9**, 1901085 (2019).
9. Shi, W., Shuai, Z. & Wang, D. Tuning thermal transport in chain-oriented conducting polymers for enhanced thermoelectric efficiency: a computational study. *Adv. Funct. Mater.* **27**, 1702847 (2017).
10. Zhang, J., Xu, W., Sheng, P., Zhao, G. & Zhu, D. Organic donor–acceptor complexes as novel organic semiconductors. *Acc. Chem. Res.* **50**, 1654–1662 (2017).
11. Park, S. K., Kim, J. H. & Park, S. Y. Organic 2D optoelectronic crystals: charge transport, emerging functions, and their design perspective. *Adv. Mater.* **30**, 1704759 (2018).
12. Ferraris, J., Cowan, D. O., Walatka, V. & Perlstein, J. H. Electron transfer in a new highly conducting donor-acceptor complex. *J. Am. Chem. Soc.* **95**, 948–949 (1973).
13. Dasari, R. R. et al. Charge-transport properties of F6TNAP-based charge-transfer cocrystals. *Adv. Funct. Mater.* **29**, 1904858 (2019).
14. Liang, Y. et al. Band engineering and majority carrier switching in isostructural donor–acceptor complexes DPTTA-FXTCNQ crystals (X = 1, 2, 4). *Adv. Sci.* **7**, 1902456 (2020).
15. Wang, D., Shi, W., Chen, J., Xi, J. & Shuai, Z. Modeling thermoelectric transport in organic materials. *Phys. Chem. Chem. Phys.* **14**, 16505–16520 (2012).
16. Shi, W., Wang, D. & Shuai, Z. High-performance organic thermoelectric materials: theoretical insights and computational design. *Adv. Electron. Mater.* **5**, 1800882 (2019).
17. Bardeen, J. & Shockley, W. Deformation potentials and mobilities in non-polar crystals. *Phys. Rev.* **80**, 72–80 (1950).
18. Brooks, H. in *Advances in Electronics and Electron Physics* (ed. Marton, L.) vol. 7 85–182 (Academic, 1955).
19. Qin, Y. et al. Efficient ambipolar transport properties in alternate stacking donor–acceptor complexes: from experiment to theory. *Phys. Chem. Chem. Phys.* **18**, 14094–14103 (2016).
20. Higashino, T. et al. Air-stable n-channel organic field-effect transistors based on charge-transfer complexes including dimethoxybenzothienobenzothiophene and tetracyanoquinodimethane derivatives. *J. Mater. Chem. C* **4**, 5981–5987 (2016).
21. Bubnova, O. et al. Optimization of the thermoelectric figure of merit in the conducting polymer poly(3,4-ethylenedioxythiophene). *Nat. Mater.* **10**, 429–433 (2011).
22. Pernstich, K. P., Rössner, B. & Batlogg, B. Field-effect-modulated Seebeck coefficient in organic semiconductors. *Nat. Mater.* **7**, 321–325 (2008).
23. Shi, W. et al. Unprecedented enhancement of thermoelectric power factor induced by pressure in small-molecule organic semiconductors. *Adv. Mater.* **31**, 1901956 (2019).
24. Kiyota, Y. et al. Benzothienobenzothiophene-based molecular conductors: high conductivity, large thermoelectric power factor, and one-dimensional instability. *J. Am. Chem. Soc.* **138**, 3920–3925 (2016).
25. Alves, H., Molinari, A. S., Xie, H. & Morpurgo, A. F. Metallic conduction at organic charge-transfer interfaces. *Nat. Mater.* **7**, 574–580 (2008).
26. Krukau, A. V., Vydrov, O. A., Izmaylov, A. F. & Scuseria, G. E. Influence of the exchange screening parameter on the performance of screened hybrid functionals. *J. Chem. Phys.* **125**, 224106 (2006).
27. Shi, W., Zhao, T., Xi, J., Wang, D. & Shuai, Z. Unravelling doping effects on PEDOT at the molecular level: from geometry to thermoelectric transport properties. *J. Am. Chem. Soc.* **137**, 12929–12938 (2015).
28. Shi, W. et al. The role of electrostatic interaction between free charge carriers and counterions in thermoelectric power factor of conducting polymers: from crystalline to polycrystalline domains. *Adv. Theory Simul.* **3**, 2000015 (2020).
29. Shi, W. et al. Poly(nickel-ethylenetetrathiolate) and its analogs: theoretical prediction of high-performance doping-free thermoelectric polymers. *J. Am. Chem. Soc.* **140**, 13200–13204 (2018).
30. Geng, H., Zheng, X., Shuai, Z., Zhu, L. & Yi, Y. Understanding the charge transport and polarities in organic donor–acceptor mixed-stack crystals: molecular insights from the super-exchange couplings. *Adv. Mater.* **27**, 1443–1449 (2015).
31. Geng, H., Zhu, L., Yi, Y., Zhu, D. & Shuai, Z. Superexchange induced charge transport in organic donor–acceptor cocrystals and copolymers: a theoretical perspective. *Chem. Mater.* **31**, 6424–6434 (2019).
32. Cheng, C., Geng, H., Yi, Y. & Shuai, Z. Super-exchange-induced high performance charge transport in donor–acceptor copolymers. *J. Mater. Chem. C.* **5**, 3247–3253 (2017).
33. Yong, X. et al. Theoretical search for high-performance thermoelectric donor–acceptor copolymers: the role of super-exchange couplings. *J. Mater. Chem. A* **8**, 21852–21861 (2020).
34. Ge, Y., Liu, R. & Shuai, Z. Abnormal Seebeck effect in doped conducting polymers. *Appl. Phys. Lett.* **118**, 123301 (2021).
35. Perdew, J. P., Burke, K. & Ernzerhof, M. Generalized gradient approximation made simple. *Phys. Rev. Lett.* **77**, 3865–3868 (1996).
36. Grimme, S., Antony, J., Ehrlich, S. & Krieg, H. A consistent and accurate ab initio parametrization of density functional dispersion correction (DFT-D) for the 94 elements H-Pu. *J. Chem. Phys.* **132**, 154104 (2010).
37. Kresse, G. & Furthmüller, J. Efficiency of ab-initio total energy calculations for metals and semiconductors using a plane-wave basis set. *Comput. Mater. Sci.* **6**, 15–50 (1996).
38. Blöchl, P. E. Projector augmented-wave method. *Phys. Rev. B* **50**, 17953–17979 (1994).
39. Tang, W., Sanville, E. & Henkelman, G. A grid-based Bader analysis algorithm without lattice bias. *J. Phys. Condens. Matter* **21**, 084204 (2009).
40. Mahan, G. D. & Sofo, J. O. The best thermoelectric. *Proc. Natl Acad. Sci. USA* **93**, 7436 (1996).
41. Shi, W., Chen, J., Xi, J., Wang, D. & Shuai, Z. Search for organic thermoelectric materials with high mobility: the case of 2,7-dialkyl[1]benzothieno[3,2-b][1]benzothiophene derivatives. *Chem. Mater.* **26**, 2669–2677 (2014).

ACKNOWLEDGEMENTS

This work was supported by the Agency for Science, Technology, and Research (A*STAR) of Singapore (1527200024 and 1527200019). Computational resources were provided by the National Supercomputing Centre Singapore (NSCC) and A*STAR Computational Resource Centre (A*CRC).

AUTHOR CONTRIBUTIONS

S.-W.Y. and G.W. designed and coordinated this study. W.S. conducted all the calculations and prepared all the figures and tables. W.S. analyzed the data and wrote the paper. T.Q.D. and Z.M.W. commented on the manuscript.

COMPETING INTERESTS

The authors declare no competing interests.

ADDITIONAL INFORMATION

Supplementary information The online version contains Supplementary Material available at https://doi.org/10.1038/s41524-021-00580-y.

Correspondence and requests for materials should be addressed to G.W. or S.-W.Y.

Reprints and permission information is available at http://www.nature.com/reprints

Publisher's note Springer Nature remains neutral with regard to jurisdictional claims in published maps and institutional affiliations.